Pressure Dependence of Current-Voltage Characteristics of a Thin Hole Hollow Cathode

Arantxa Danielle S. MONTALLANA,* Magdaleno R. VASQUEZ, Jr.,** and Motoi WADA*

(Received October 3, 2023)

The use of plasma technology is an established technique for the synthesis of Ag-TiO_2 nanostructures. However, Ag-TiO_2 formation often involves several steps and different plasma sources. In this work, a Ti hollow cathode electrode with a 0.7 mm aperture was designed to examine its performance in Ar discharge production and its potential as a sputter source for the formation of TiO_2. The electrode demonstrated excellent stability against high-voltage break down and was able to sustain Ar discharge in the pressure range from 10 to 100 Pa. The steady state production of metallic particle flux is expected with enough cathode voltage to ensure a necessary sputtering yield. The source can generate the sputtered atom flux of the order of one monolayer per second and can serve as the Ti source for TiO_2 atomic layer film preparation. After establishing the cathode performance in Ar, the compatibility of the addition of oxygen and vaporized Ag metal precursor to the discharge carrier gas will be investigated and the versatility of the thin-hole electrode for Ag-TiO_2 heterostructure formation will be confirmed.

Keywords: plasma process, hollow cathode, TiO_2

1. Introduction

Surface nanostructures or nanometer scale structures often reveal specifically useful functions. Particularly, noble metal-coupled oxides exhibit some desirable features compared with homogeneously coated counterparts due to the larger surface density of active sites leading to higher catalytic performance.[1)] An example is silver-titanium dioxide (Ag-TiO_2) nanostructures, which exhibit unique functional properties and potential applications in medicine,[2)] self-cleaning coatings,[3)] photocatalysis[4)] and others.

Advances in engineering TiO_2 into different configurations, size, and functionality have been done to maximize its catalytic properties.[5-6)] Coupling noble metals onto TiO_2 surface have been reported to enhance photocatalytic reaction, which is attributed to the formation of a Schottky barrier due to the difference in their work function. The noble metal acts as an electron trap, which reduces the recombination rate of the electron-hole pairs.[8)] Among the noble metals that can be incorporated or coupled with TiO_2 is Ag.[7,8)] Methods to synthesize Ag-TiO_2 nanostructures include impregnation,[9)] sol-gel,[10)] hydrothermal[11)] and photo deposition processes.[12)] However, these synthesis processes often involve the usage of harmful chemical reducing agents and high operating temperatures. Therefore, alternative reduction methods that are safer and environmentally friendly have been explored.[13)]

One possible way to achieve a desired chemical reaction is through electron-based metal ion reduction methods.[14)] The methods include electron beam irradiation[15-19)] and electron-assisted reduction using glow discharge plasmas as the source of electrons.[4, 20, 21)] Due to the dynamic

*Graduate School of Science and Engineering, Doshisha University, Kyotanabe Kyoto
Telephone : +81-774-65-6349, E-mail : cyjg2301@mail4.doshisha.ac.jp, mwada@mail.doshisha.ac.jp
**Department of Mining, Metallurgical, and Materials Engineering, College of Engineering, University of the Philippines, Diliman, Quezon City, Philippines
Telephone : +63-928-552-6554, E-mail : mrvasquez2@up.edu.ph

nature of plasma, the mechanisms responsible for these reduction reaction processes require further fundamental study based on a detailed investigation of electron energy distribution function right at the reaction sites and the characterization of electrons and other active species within cold plasmas.[14)]

We have been working on the investigation of plasma-based reduction processes for converting Ag compound ($AgNO_{3(aq)}$) to metallic Ag on the surface of TiO_2. These plasma-induced reduction methods involve the use of glow discharge[4)] and broad low energy electron beam for constructing an Ag-TiO_2 heterostructure. In this work, we explored the discharge characteristics of a thin-hole hollow cathode and its potential as a synthesis route for Ag-TiO_2 nanostructure formation.

2. Experimental Approach

A vacuum system that enables testing of different types of plasma excitation has been designed and assembled for the experiment. The discharge cathode should serve as a particle source for sputter-deposition of Ti thin layer.

2.1. *Experimental Apparatus*

Figure 1 describes the experimental arrangement showing the cross-sectional view of the experimental apparatus. The vacuum chamber accommodates a 165 mm diameter 120 mm high cylindrical volume pumped down by a 50 l/s turbo-molecular pump evacuated by a 24 l/min oil rotary pump. The device equips a rotatable target holder that can hold targets at any distance from the cathode end. A 10 mm thick glass plate enables the observation of plasma from the top of the chamber. The cathode, with the detailed structure shown in Fig. 2, holds the sputtering target having a thin hole of 12 mm long with the 0.7, 0.8 or 1.0 mm diameter as the discharge gas conduit for maintaining a stable plasma. The actual material of the sputtering target is Ti, while the test pieces for the discharge characteristics measurements are made of stainless steel. A metal plate simulating a film deposition target is placed 50 mm above the discharge cathode to measure the electrical current at the ground potential.

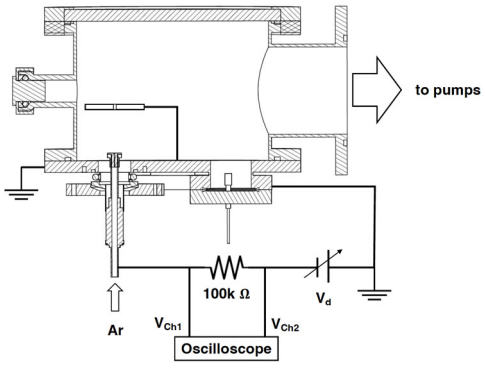

Fig. 1. Experimental arrangement for testing the thin-hole discharge cathode performance.

A 1 kV, 1 A discharge power supply ignites the plasma between the thin-hole hollow cathode and the electrically grounded test chamber serving as the anode of a discharge. A 100 kΩ ballast resistor stabilizes the discharge by the negative feedback due to the voltage drop proportional to the discharge current. A pair of 100:1 high-voltage probes measure the voltage drop across the ballast resistor to determine the discharge current and voltage.

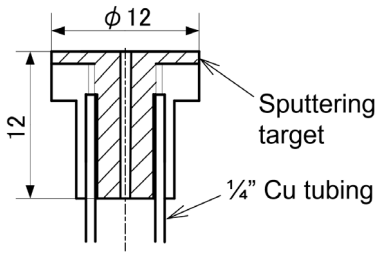

Fig. 2. The structure and dimensions of the thin-hole hollow cathode electrode.

2.2. *Experimental Procedure*

A continuous evacuation of the system with the turbo-molecular pump brings the system pressure down to $2.0X10^{-4}$ Pa. After confirming the system reaches the background pressure with a quartz-type vacuum gauge, a needle valve attached to the end of the 1/4 inch (6.35 mm) diameter stainless-steel tube holding the thin-hole cathode regulates the argon (Ar) gas flow to control the pressure inside of the chamber. The flow rate adjustment by the

needle valve realized a steady state plasma operation in the Ar pressure ranges from 10 to 100 Pa.

Slow increase of power supply voltage commenced a discharge with the discharge current between the thin-hole cathode and chamber wall anode. The discharge current increased with increasing discharge voltage up to about 760 V determined from the voltage limit of the power supply and the voltage drop across the ballast resistor. A three-channel oscilloscope measured the discharge voltage, the electrode voltage, and the voltage excited to the target simulating electrode. Discharge current and discharge voltage characteristics were measured by keeping a constant Ar pressure.

3. Experimental Result

An image of typical discharge created by the thin-hole hollow cathode shown in Fig. 3 indicates the concentration of dense plasma around the region of the gas channel. The front surface of the electrode should work as the sputtering source: Ti for our application purpose. Due to the design structure, the side wall of the cathode can also generate electrons that increase discharge current. A strong magnetic field (~ 1 kG) produced by permanent magnets can diminish this part of electron emission from the cathode, but the magnets were removed from the system to observe the discharge characteristics for a wide range of pressure.

3.1. *Current Voltage Characteristics*

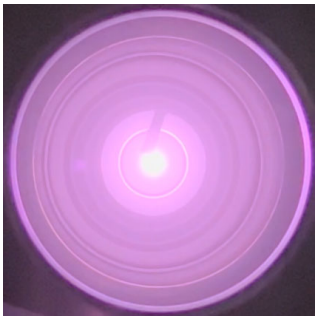

Fig. 3. Image of plasma glow observed around the thin-hole hollow cathode.

Figure 4 shows a typical discharge current voltage characteristics of the thin-hole hollow cathode discharge. As the applied voltage exceeds the ignition threshold, the discharge current reaches a constant value keeping the electrode voltage much higher than the ionization potential of Ar. At any Ar pressure from 10 to 100 Pa, the discharge current increased with the increasing discharge voltage to exhibit a normal glow discharge characteristic.

The region where the alpha effects or the ionization events predominates seems concentrated near the electrode hole. In the hollow discharge mode, the plasma density must be high enough to make the sheath thickness smaller than the hole diameter. The picture in Fig. 3 shows a bright glow centered at the electrode hole, and frequent ionization is expected around the area, making the local ion density as the result of frequent ionization collisions.

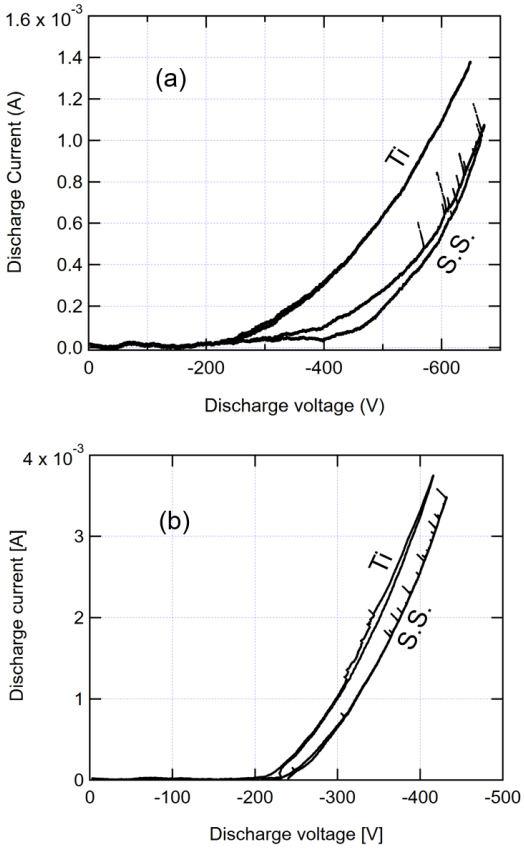

Fig. 4. Discharge current-voltage characteristics of Ti and stainless steel thin-hole hollow discharge cathodes when the chamber pressure was (a) 30 Pa, and (b) 100Pa.

Furthermore, these ionization events produce more electrons and other energetic species interacting with the surface of the cathode, thereby increasing the probability of secondary electron emission. The higher discharge current measured for the Ti cathode as observed in Fig. 4 may be attributed to having a higher secondary electron yield compared to stainless steel.

3.2. *Current Signal at the Remote Electrode*

The voltage excited across a 100 kΩ resistor connecting a remote electrode working as a simulation deposition target to the ground was measured while the discharge voltage was scanned for varying Ar gas pressure. The results compiled in Fig. 5 show the signal dependence upon the discharge voltage similar to the discharge current-voltage characteristics. The signal was found smaller for higher pressure operations than for operations with lower pressures. Particularly, the characteristics showed a change from saturating behavior to increasing behavior against the voltage increase as the pressure was raised above 30 Pa. The hole size did not affect the signal intensity as the diameter of the hollow cathode hole was increased from 0.7 mm to 1.0 mm diameter. The signal stayed constant independent of the hole diameter, while a small increase in signal intensity was observed for smaller diameter electrode.

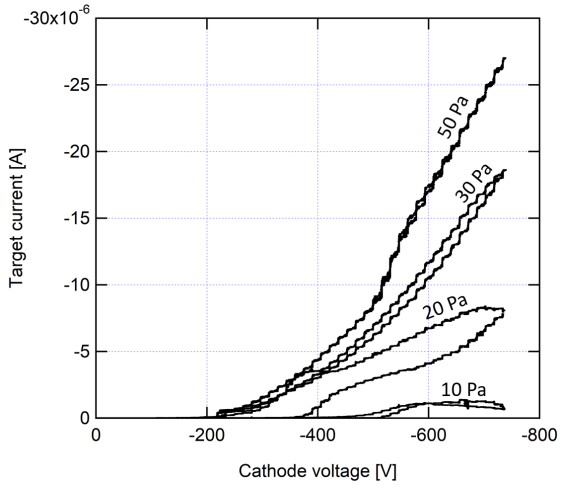

Fig. 5. Current signal dependence upon the discharge voltage at varying operating pressures.

4. Discussion

4.1. *Estimation of Ion flux*

The observation of plasma glow inside of the thin-hole suggests the Debye shielding length λ_d given by,

$$\lambda_d = \sqrt{\frac{\epsilon_0 k_B T_e}{e^2 n_e}} \quad (1)$$

where ϵ_0: vacuum permittivity, k_B: Boltzmann constant, T_e: electron temperature, e: unit charge and n_e: electron density, can be smaller than the hole diameter. For typical value of T_e ~ 5 eV, the diameter λ_d can be less than 1 mm for electron density n_e > 3×10^{10} cm^{-3}, which can be easily realized in an ordinary glow discharge.

The density downstream of the electron acceleration sheath can be estimated through the equation of continuity with the ion flux ϕ_{ion} determined by the downstream electron temperature T_d and downstream electron density n_d for ion mass M_i.

$$\phi_{ion} = \frac{1}{2} n_d \sqrt{\frac{k_B T_d}{M_i}} \quad (2)$$

Here, the factor $e^{-\frac{1}{2}}$ which is usually used to account for the formation of presheath was replaced with the round number 1/2. Assuming 5 eV temperature with 750 eV electron extraction potential, the plasma density should be one order of magnitude smaller than the density inside the hollow cathode discharge. With 10^9 cm^{-3} estimated electron density and 1 eV electron temperature of the plasma across the cathode sheath, the Ar ion flux to the cathode is about 1.5×10^{14} cm^{-2}s^{-1}.

4.2. *Expected performance as a flux source*

The estimated flux of the order of 10^{14} cm^{-2}s^{-1} approximately corresponds to one monolayer per second. From the surface of the sputtering target, sputtered material atoms direct toward the deposition target with the flux at the source surface with the amount multiplying the incident singly charged Ar (Ar$^+$) ion flux by the sputtering yield at the energy of the incident Ar$^+$ ions. The result of Ti sputtering yield computed with Yamamura formula[22]

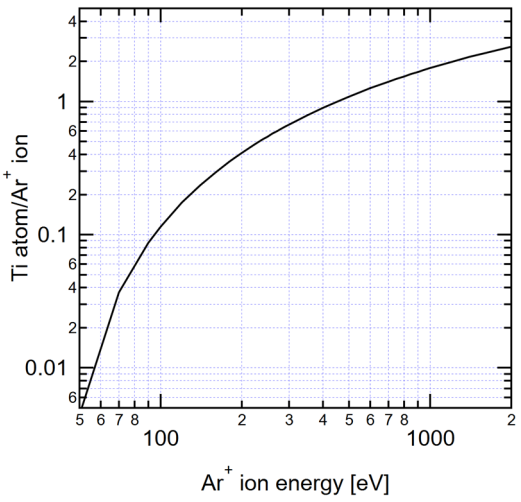

Fig. 6. Sputtering yield of Ti plotted as a function of incident energy of Ar^+ ions.

plotted as the function of Ar ion incident energy is shown in Fig. 6. In the energy range above 500 eV, the sputtering yield exceeds unity corresponding to the Ti atom flux equivalent to the incoming Ar ion flux.Due to geometrical constraints, this particle flux can reduce one to two orders of magnitude at the deposition target surface.

4.3. *Performance improvement by magnetic field.*

The present design of the cathode allows the direct discharge current flow from the side of the cathode. This should enlarge the power required to sustain the discharge,

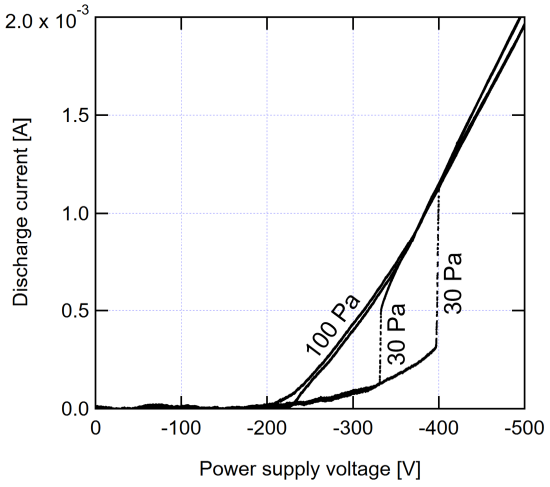

Fig. 7. Discharge characteristics with the linear magnetic field induced to the thin-hole hollow cathode.

but the plasma production in the surrounding area should enhance the stability of the ion current striking the sputtering target surface. One way to increase the ion density at the sputtering target is to induce a linear magnetic field along the axis of the thin-hole hollow cathode. To see the effect due to a linear magnetic field, a Nd-Fe ring manet (59 mm O.D. 43 mm I.D. 14 mm thick) was placed on the vacuum flange supporting the cathode. The result of the discharge characteristics for a 0.7 mm hole Ti cathode is depicted in Fig. 7.

Characteristics at 30 Pa and 100 Pa pressure are shown in Fig. 7 to compare with the magnetic field free condition shown in Fig. 4. The abscissa plots the power supply voltage instead of the discharge voltage to elucidate clear onsets of discharge ignition and extinction: hysteresis loops. As evident from the comparison between graphs, the discharge current at a lower operating pressure increased by the induction of the linear magnetic field. Further optimization of the magnets arrangement may increase the efficiency to couple discharge power to the ion flux onto the targe surface and the design modifications of the discharge system will be made on the obtained results.

5. Conclusions

Thin-hole hollow cathode electrode as the sputter source of metallic element was designed and examined the performance for Ar discharge gas. The designed electrode demonstrated excellent stability against high-voltage breakdown, and steady state production of metallic particle flux is expected with enough cathode voltage to ensure a necessary sputtering yield. The source can generate the sputtered atom flux of the order of one monolayer per second and can serve as the Ti source for TiO_2 atomic layer film preparation. The compatibility with oxygen addition to the discharge gas must be confirmed before the complete Ag-TiO_2 nanostructure production system will be finalized.

The discharge condition monitoring by an electrode insertion can be an easy way to control the operation of the

film deposition system. The system performance will be further improved with the permanent magnet arrangement for optimizing system efficiency while precisely controlling the discharge parameters.

This work was supported in part by grants-in-aid for division research from the Harris Science Research Institute of Doshisha University. It was also supported in part by the Japan Society for the Promotion of Science KAKENHI No. 23H01158.

References

1) H. H. Kim, Y. Teramoto, A. Ogata, H. Takagi, and T. Nanba, "Plasma Catalysis for Environmental Treatment and Energy Applications", *Plasma Chemistry and Plasma Processing,* **36,** 45-47 (2016).
2) S. A. H. Jalali, A. R. Allafchian, S. S. Banifatemi, and A. Ashrafi Tamai, "The antibacterial properties of Ag/TiO_2 nanoparticles embedded in silane sol-gel matrix", *Journal of the Taiwan Institute of Chemical Engineers,* **66,** 357-362 (2016).
3) X. H. Yang, H. T. Fu, X. C. Wang, J. L. Yang, X. C. Jiang, and A. B. Yu, "Synthesis of silver-titanium dioxide nanocomposites for antimicrobial applications", *Journal of Nanoparticle Research,* **16,** 2526 (2014).
4) A. D. Montallana, J. P. Angeles, J. P. Chu, M. Sherburne, M. Vasquez, and M. Wada, "Fabrication of plasma-reduced silver coupled with titanium dioxide nanoparticles for visible ligh-driven photocatalysis", *Journal of Vacuum Science & Technology B,* **41,** 042204 (2023).
5) S. Dong, J. Feng, M. Fan, Y. Pi, L. Hu, X. Han, M. Liu, J. Sun, and J. Sun, "Recent developments in heterogeneous photocatalytic water treatment using visible light-responsive photocataysts: a review", *RSC Adv*ances, **5,** 14610-14630 (2015).
6) P. Kamat, "Semiconductor Surface Chemistry as Holy Grail in Photocatalysis and Photovoltaics", *Accounts of Chemical Research,* **50,** 527-531 (2017).
7) A. Chauhan, M. Rastogi, P. Scheier, C. Bowen, R. V. Kumar, and R. Vaish, "Janus nanostructures for heterogeneous photocatalysis", *Applied Physics Reviews,* **5,** 041111 (2018).
8) R. Goei and T. Lim, "Ag-decorated TiO_2 photocatalytic membrane with hierarchical architecture: Photocatalytic and antibacterial activities", *Water Research,* **59,** 207–218 (2014).
9) B. Naik, C. Manoratne, A. Chandrashekhar, A. Iyer, V. Prasad, and N. Ghosh, "Preparation of TiO_2, Ag-doped TiO_2 nanoparticle and TiO_2-SBA-15 nanocomposites using simple aqueous solution-based chemical method and study of their photocatalytical activity", *Journal of Experimental Nanoscience,* **8,** 462-479 (2013).
10) S. Abbad, K. Guergouri, S. Gazaout, S. Djebabra, A. Zertal, R. Barille, and M. Zaabat, "Effect of silver doping on the photocatalytic activity of TiO_2 nanopowders synthesized by the sol-gel route", *Journal of Environmental Chemical Engineering,* **8,** 103718 (2020).
11) X. Zheng, D. Zhang, Y. Gao, Y. Wu, Q. Liu, and X. Zhu, "Synthesis and characterization of cubic Ag/TiO2 nanocomposites for the photocatalytic degradation of methyl orange in aqueous solutions", *Inorganic Chemistry Communications,* **110,** 107589 (2019).
12) K. Wenderich and Guido Mul, "Methods, Mechanism, and Applications of Photodeposition in Photocatalysis: A Review", *Chemical Reviews,* **116**[23], 14587-14619 (2016).
13) R. White, R. Luque, V. Budarin, J. Clark, and D. Macquarrie, "Supported metal nanoparticles on porous materials. Methods and applications", *Chemical Society Reviews,* **38**[2], 481-494 (2009).
14) C. Liu, M. Li, J. Wang, X. Zhou, Q. Guo, J. Yan, and Y. Li, "Plasma methods for preparing green catalysts: current status and perspective", *Chinese Journal of Catalysis,* **37**[3], 340-348 (2016).
15) Y. Ohkubo, Y. Hamaguchi, S. Seino, T. Nakagawa, S. Kageyama, J. Kugai, H. Nitani, K. Ueno, and T. Yamamoto, "Preparation of carbon-supported PtCo nanoparticle catalysts for the oxygen reduction reaction in polymer electrolyte fuel cells by an electron-beam irradiation reduction method", *Journal of Materials Science,* **48,** 5047-5054 (2013).
16) S. Seino, T. Kinoshita, T. Nakagawa, T. Kojima, R. Taniguci, S. Okuda, and T. Yamamoto, "Radiation induced synthesis of gold/iron-oxide composite nanoparticles using high-energy electron beam", *Journal of Nanoparticle Research,* **10,** 1071-1076 (2008).
17) Y. Pai, H. Huang, Y. Chang, C. Chou, F. Shiue, "Electron-beam reduction method for preparing electrocatalytic particles for membrane electrode assemblies (MEA)", *Journal of Power Sources,* **159**[2], 878-884 (2006).
18) K. Song, D. Sauter, J. Wu, V. Dravid, and P. Stair, "Evolution of High-Energy Electron Beam Irradiation Effects on Zeolite Supported Catalyst: Metal Nanoprecipitation", *ACS Catalysis,* **2**[3], 384-390 (2012).
19) J. Kugai, T. Moriya, S. Seino, T. Nakagawa, Y. Ohkubo, H. Nitani, Y. Mizukoshi, and T. Yamamoto, "Effect of support for Pt-Cu bimetallic catalysts synthesized by electron beam irradiation method on preferential CO oxidation", *Applied Catalysis B: Environmental,* **126,** 306-314 (2012).
20) J. Zou, Y. Zhang, and C. Liu, "Reduction of Supported Noble-Metal Ions Using Glow Discharge Plasma", *Langmuir,* **22**[26], 11388-11394 (2006).
21) M. Darwish, C. Gonzalez, B. Kolenovic, A. Deremer, D. Centeno, T. Liu, D. Kim, T. Cattabiani, T. Drwiega, I. Kumar, C. Li, and C. Traba, "Rapid synthesis of metal nanoparticles using low-temperature, low-pressure argon plasma chemistry and self-assembly", *Green Chemistry* **24**[20], 8142-8154 (2022).
22) N. Matsunami, Y. Yamamura, Y. Itikawa, N. Itoh, Y. Kazumata, S. Miyagawa, K. Morita, R. Shimizu, and H. Tawara, "Energy Dependence of the Yields of Ion-induced

Sputtering of Monatomic Solids", (Institute of Plasma Physics, Nagoya, 1983), IPPJ-AM-32.